

Cite this: *J. Mater. Chem. A*, 2019, 7, 12833

Mapping the frontiers of quinone stability in aqueous media: implications for organic aqueous redox flow batteries†

Daniel P. Tabor,^{‡a} Rafael Gómez-Bombarelli,^{‡§a} Liuchuan Tong,^{‡a} Roy G. Gordon,^{‡ab} Michael J. Aziz^{‡b} and Alán Aspuru-Guzik^{‡*acd}

Quinone–hydroquinone pairs have been proposed as biologically-inspired, low-cost redox couples for organic electrolytes for electrical energy storage, particularly in aqueous redox flow batteries. In their oxidized form, quinones are electrophiles that can react with the nucleophilic water solvent resulting in loss of active electrolyte. Here we study two mechanisms of nucleophilic addition of water, one reversible and one irreversible, that limit quinone performance in practical flow batteries. Using a combination of density functional theory and semi-empirical calculations, we have quantified the source of the instability of quinones in water, and explored the relationships between chemical structure, electrochemical reduction potential, and decomposition or instability mechanisms. The importance of these mechanisms was further verified through experimental characterization of a family of alizarin-derived quinones. Finally, ~140 000 prospective quinone pairs (over 1 000 000 calculations including decomposition products) were analyzed in a virtual screening using the learned design principles. Our conclusions suggest that numerous low reduction potential molecules are stable with respect to nucleophilic addition, but promising high reduction potential molecules are much rarer. This latter fact suggests the existence of a stability cliff for this family of quinone-based organic molecules, which challenges the development of all-quinone aqueous redox flow batteries.

Received 25th March 2019
Accepted 3rd May 2019

DOI: 10.1039/c9ta03219c

rsc.li/materials-a

1 Introduction

Flow batteries could help solve the intermittency problem of wind and solar renewable sources by storing electrical energy in fluids in scalable external storage tanks. Research into low-cost alternatives to current-standard vanadium electrolytes has exploded in the past five years, with organic, inorganic, and

organometallic electrolytes developed for both aqueous and non-aqueous systems.^{1–19} For aqueous flow batteries, the vast majority of developments have been new molecules for the low reduction potential electrolyte (the negolyte), with the molecule for the high-potential electrolyte (the posolyte) serving as a greater challenge. Some success has been found using single-electron couples at neutral and high-pH.^{3–5,9,10} Initial work in acidic aqueous metal-free flow batteries used bromine as the posolyte active species² and two recent studies used benzoquinone-based molecules.^{6,8} However, the maximum standard reduction potential for an acidic organic posolyte that has lasted even a few cycles (3,6-dihydroxy-2,4-dimethylbenzene sulfonic acid or DHDMBS) is only 0.85 V vs. the standard hydrogen electrode (SHE)—this is almost 0.4 V below the thermodynamic threshold for evolving oxygen.⁸ In addition to the need to develop high potential molecules, there is also interest in developing single molecules with three distinct, well separated (>1.0 V) redox states, that could potentially serve in both posolyte and negolyte. Discovering molecules with this property could enable flow batteries that replace the ion-selective membrane with an inexpensive porous separator.^{20–22} One potential three-redox-state molecule is a fused quinone, which contains four total ketone groups.

A primary concern in developing flow battery electrolytes is their chemical and electrochemical stability. Organic molecules

^aDepartment of Chemistry and Chemical Biology, Harvard University, Cambridge, MA 02138, USA. E-mail: alan@aspuru.com

^bHarvard John A. Paulson School of Engineering and Applied Sciences, Cambridge, Massachusetts 02138, USA

^cDepartment of Chemistry and Department of Computer Science, University of Toronto, Toronto, Ontario M5S 3H6, Canada

^dVector Institute, Toronto, ON M5G 1M1, Canada

† Electronic supplementary information (ESI) available: The ESI contains plots showing the calibration of the reduction potential and $\log K_{\text{hyd}}$ at different levels of electronic structure theory, the raw data that are used to calibrate the reduction potential and $\log K_{\text{hyd}}$, CVs and the calculated thermodynamic stability of the alizarin family, the synthesis and NMR stability study of quinizarin, lists of high-potential molecules that pass various stability criteria, results of screening from stricter stability criteria, and a scheme for a potential ring-opening mechanism not fully explored in this paper. See DOI: 10.1039/c9ta03219c

‡ These authors contributed equally to this work.

§ Present address: Department of Materials Science and Engineering, Massachusetts Institute of Technology, Cambridge, MA 02139, USA.

are subject to a variety of decomposition reactions, which vary across different backbones, functionalizations, and environments. Reactions involving quinones, as both reactants and catalysts, have long been of interest to chemists for both fundamental and industrial reasons.²³ Researchers interested in employing quinones in aqueous flow batteries have investigated the susceptibility of low potential quinones to reactions with bromine in acid²⁴ and anthrone formation in base.²⁵ A Michael-addition mechanism has been proposed for their reactions with water.^{6,8,20}

Here, we present a virtual screening of quinone space to quantify the thermodynamic susceptibility of quinones to decomposition reactions with water. We constructed a comprehensive library of quinone-derived molecules (with backbones shown in Fig. 1A), containing 146 857 hydroquinone pairs and associated products from reactions.^{4,26,27} The targets are high reduction potential and high thermodynamic stability with respect to water attack. Some high potential molecules, such as tiron, have been previously shown to undergo a Michael reaction in the literature and the calculated susceptibility can serve as a rough cutoff to use in screening. For this work, we experimentally characterized a family of alizarin derivatives (structures shown Table S3[†]) with high reduction potential to verify that these mechanisms transfer from benzoquinones to anthraquinones and gain some further information on what thermodynamic cutoffs to use in our virtual screening. These results, taken together, show the

tradeoffs between achieving a high reduction potential quinone and maintaining long-term stability.

2 Results and discussion

The molecular backbones and mechanisms of decomposition reactions that we considered are summarized in Fig. 1. The two-proton two-electron redox activity of a molecule (Fig. 1B) can be kinetically inhibited by the formation of a *gem*-diol (Fig. 1C) and the molecule can undergo chemical degradation through a Michael addition or substitution reaction (Fig. 1D).

2.1 Reduction potential structure–property relationships

The choice of candidate quinone pool was based on previous reports,²⁶ where molecular motifs more likely to give high reduction potentials and high solubility have been identified. The molecules were generated as fully reduced parts of redox pairs and subject to two-proton, two-electron oxidation reactions. The reduction potentials are calculated at the calibrated PM7 COSMO level of theory.^{28,29} Details on the calibration procedure and the calibration results for higher levels of theory are given at the end of the manuscript and in the ESI (Fig. S1[†]). The parity between the DFT and PM7 COSMO results on the calibration set enabled the computation of all of the properties of the molecules within this large chemical space. For hydroquinones with multiple potential oxidation patterns, all

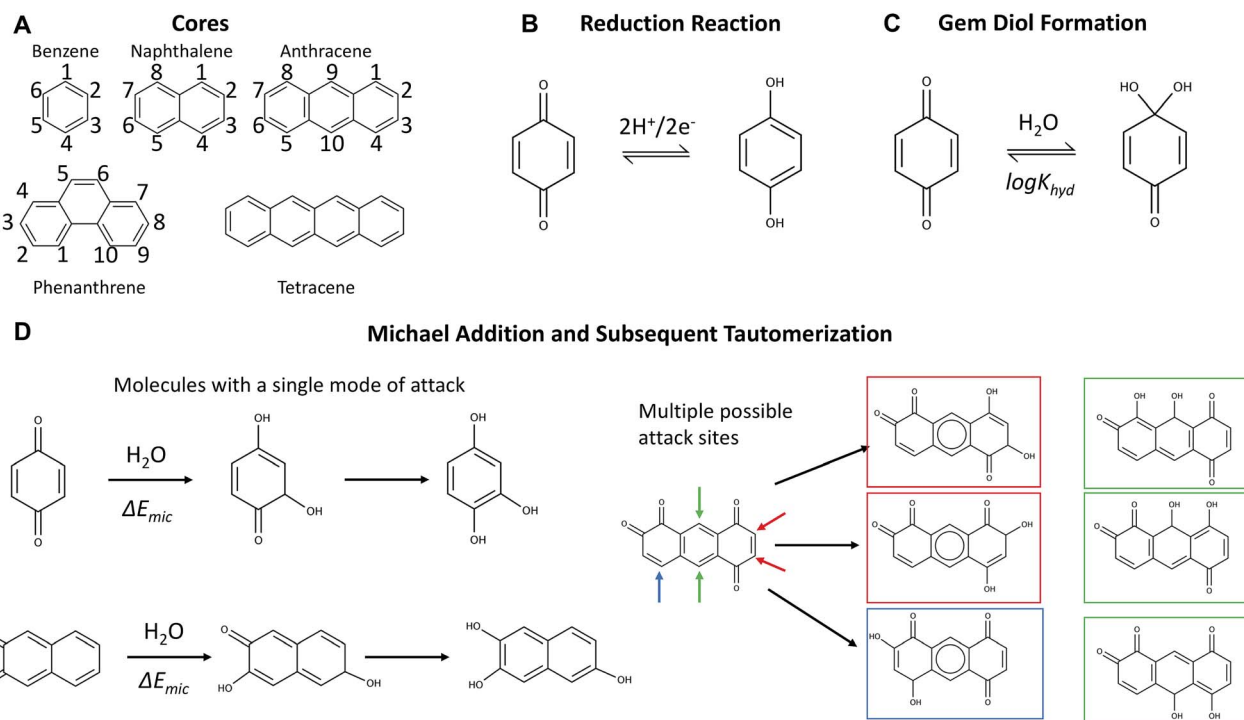


Fig. 1 (A) All backbones (without oxidation topologies indicated) considered in this study. The molecules discussed in detail are labeled to give a short description of the redox-active sites in a given molecule. (B) The redox reaction of quinones in acidic aqueous flow batteries: the two-proton two-electron reduction of two ketones to two hydroxyl groups (C) mechanism for *gem*-diol formation, which is reversible but hampers kinetics. (D) Illustrations of Michael addition (irreversible) on molecules with a single vulnerable site (with subsequent tautomerization shown) and on molecules with multiple vulnerable attack sites. Michael addition can also occur on substituted sites, where it becomes a substitution reaction.

mechanisms have been considered, and results are reported for the reaction with the highest thermodynamic driving force.

Fig. 2 plots the distribution of the calculated reduction potentials *vs.* SHE at pH = 0 for the benzoquinones, naphthoquinones, anthraquinones, and phenanthrene-functionalized quinones across the three main functional groups considered in this study: carboxylic acids, sulfonic acids, and phosphonic acids. Within each distribution, there are variations in the hydroxyl substitutions for the non redox-active parts of the molecules and the number and positioning of the other functional groups. In general, the redox pattern, also referred to as the relative positions of the redox-active hydroxyl groups, has the strongest influence over reduction potential; this is most easily seen by examining the median values in Fig. 2. The choice of electron withdrawing group has a slightly weaker effect, particularly for the larger backbones. Also of note is that essentially every redox pattern and functional group combination is capable of producing quinones with both high potentials (near ~ 1.00 V) and low potentials (~ 0.1 V). Overall, the theoretical methods predict that carboxylic acid and sulfonic acid functionalizations lead to higher reduction potentials within a given redox-active pattern.

For the benzoquinones (Fig. 2A) and naphthoquinones (Fig. 2B), there is not as large of a difference between the medians of the different redox-active patterns as there are for the anthraquinones (Fig. 2C) and phenanthrene-functionalized

quinones (Fig. 2D). In the former two cases, the functional groups are much more likely to be close to the redox-active sites of the molecules and thus appear to have a more pronounced effect on the reduction potential. For the two three-ring families of molecules, we see that certain reduction patterns consistently produce higher distributions with 1-7 and 2-3 for anthraquinones and 3-5, 2-3, and 1-10 for the phenanthrene-functionalized quinones.

2.2 Relationship between reduction potential and water stability: computational results

Having established the structure-property relationships between the quinone functionalization and reduction potential, the relationship between the reduction potential and thermodynamic stability criteria was explored. Two metrics of susceptibility related to the addition of water were considered: $\log K_{\text{hyd}}$ (the calculated base-10 logarithm) and ΔE_{mic} for a reversible *gem*-diol formation (Fig. 1C) and irreversible Michael addition/substitution (Fig. 1D), respectively. The calibration results for the calculation of $\log K_{\text{hyd}}$ are in Fig. S2.† The thermodynamic susceptibility to Michael addition is calculated from the initial reaction in Fig. 1D to form a high-energy tetrahedral intermediate that breaks aromaticity, which according to Hammond's postulate, should most bear the most similarity to the transition state associated with this reaction across the library of

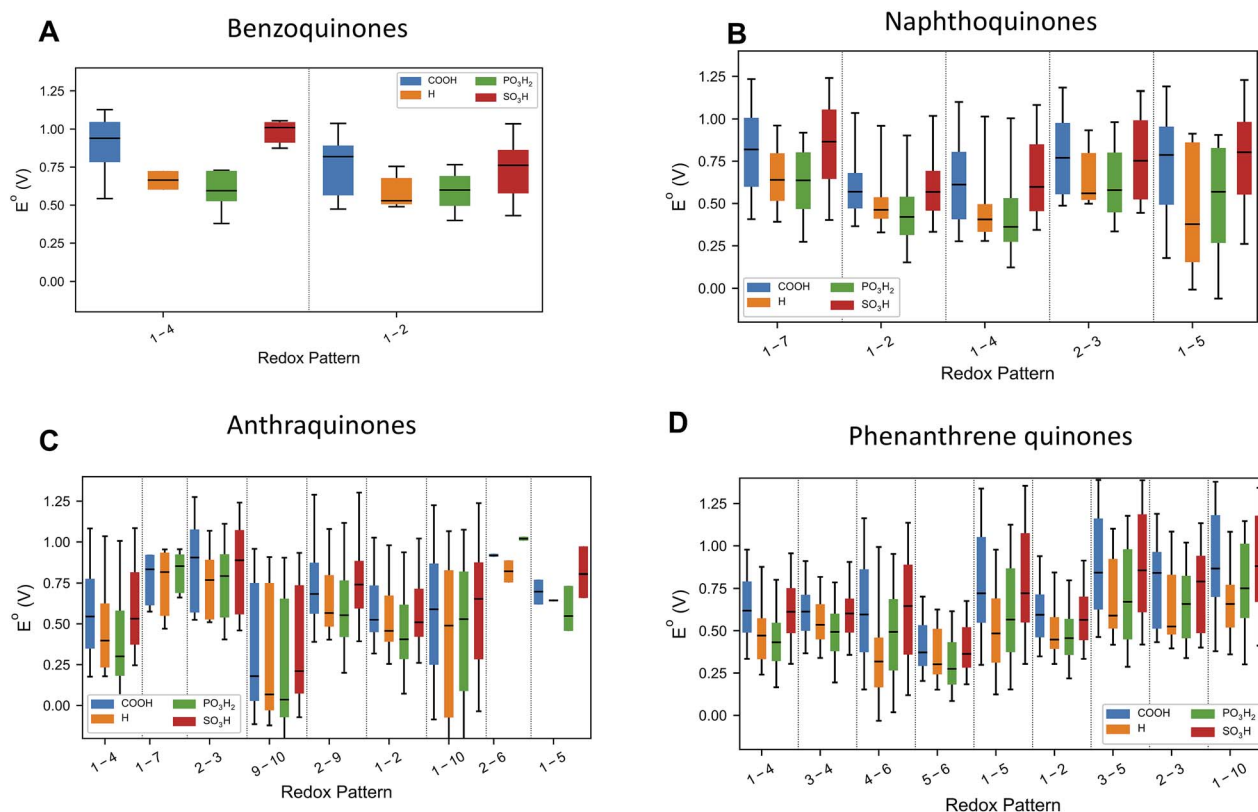


Fig. 2 Reduction potential dependence on both relative ketone positions and functional groups. The numbers refer to the topology of the redox-active ketones and correspond to the labels in Fig. 1. The median of each set of data is indicated with a black line. The regions bounded by the colors indicate the range of the 5th and 95th percentile of reduction potentials. The lines extend out to the maximum and minimum reduction potential for each substitution and ketone topology.

quinones. Though we do not have a calibration set for these Michael addition energies, we can compare molecules within the library to each other for relative fitness. Chemical principles suggest that as molecules become more electron-deficient, both the reduction potential would increase and so would the electrophilicity, thus increasing the susceptibility to nucleophilic attack from a species like water.

The quinone molecules were divided into two groups, motivated by the possibility of discovering a fused-quinone with three separated redox states. Note that in all cases, the fully reduced hydroquinone, which has no ketone groups, is subject to neither *gem*-diol formation nor the Michael addition. The first group includes quinones that have only a single two-proton two-electron oxidation (referred to in shorthand as SO – single oxidation) from its fully reduced form. The second group involves quinones that are the products of a subsequent second oxidation (referred to as DO – double oxidation), which means that the oxidized products have four ketone groups. Fig. 3A and B show the calculated $\log K_{\text{hyd}}$ of the SO and DO oxidized forms of the pairs, respectively, and Fig. 3C and D show the same for the Michael addition/substitution energy. We define Michael addition/substitution energy as

$$\Delta E_{\text{mic}} = (E(\text{oxidized}) + E(\text{H}_2\text{O}) - E(\text{Michael product})) \quad (1)$$

where the water energy is evaluated for a single water molecule.

For the first oxidation (SO group), the thermodynamic favorability of nucleophilic attack by water increases with the reduction potential of the molecule (Fig. 3A and C). This is consistent with the chemical principles argument outlined above that the more electron deficient core will have both a higher reduction potential and be more susceptible to Michael addition. However, for the second two-proton two-electron oxidations, the correlation between both $\log K_{\text{hyd}}$ and ΔE_{mic} and the reduction potential is substantially less pronounced, indicating that all fused quinones in their fully oxidized state are relatively electron deficient, or at least have an electron deficient spatial region, in terms of having a vulnerable site for water attack. This implies that the development of a fused quinone that is stable is more challenging than a high reduction potential molecule with the same reduction potential.

2.3 Experimental investigation of fused quinone stability

A family of fused quinones was investigated experimentally to both test the validity of the computational studies and also

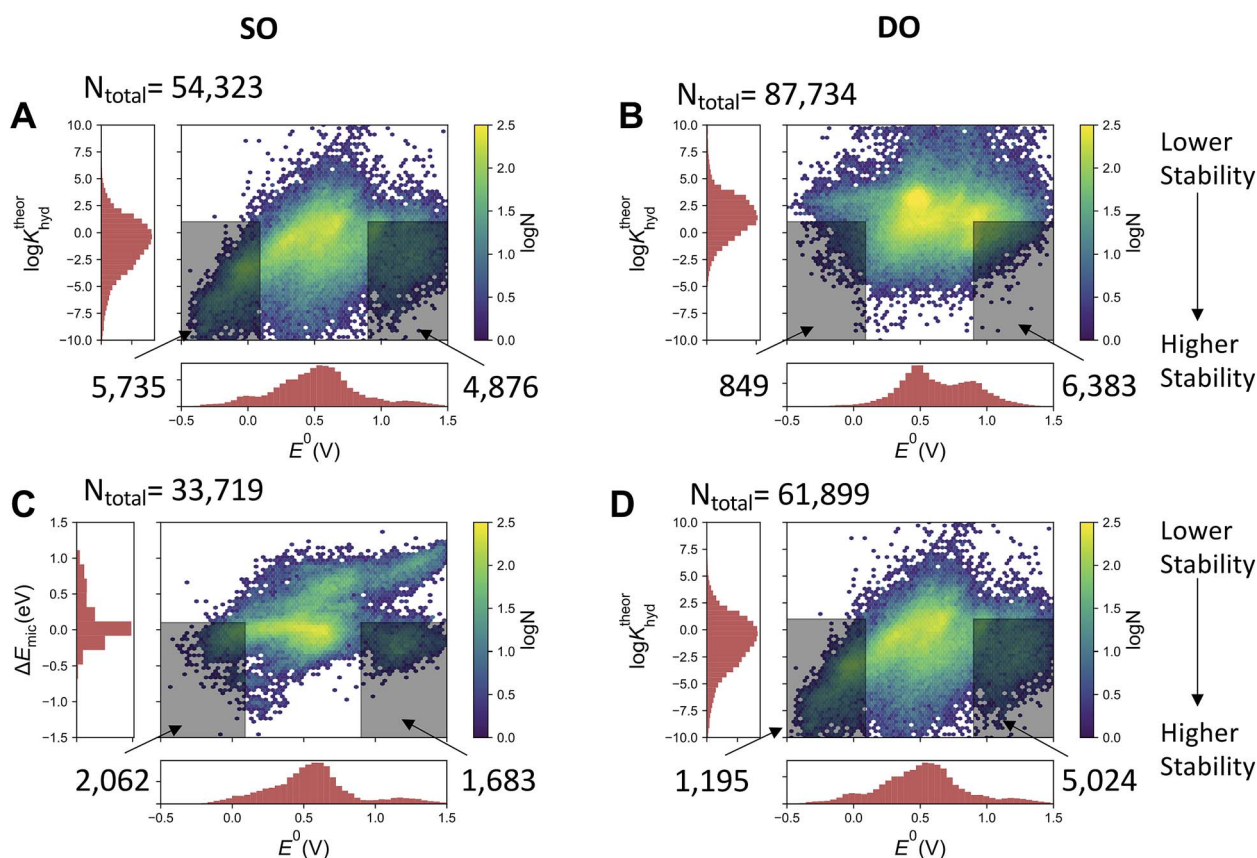


Fig. 3 Correlations between calculated nucleophilic attack susceptibility and half-cell reduction potential for quinone-hydroquinone pairs. The quinone pairs are divided into two groups. The SO group contains pairs of molecules where a fully reduced hydroquinone is oxidized through a single two-proton two-electron oxidation to a quinone. The DO group contains pairs of singly two-proton two-electron oxidized quinones that may undergo a second two-proton two-electron oxidation process. N_{total} indicates the number of molecules in each plot. Shaded regions indicate molecules that have both satisfactory reduction potentials to be viable negolytes or posolytes and have relatively high thermodynamic stability with respect to the specified reaction with water.

provide guidance for what cutoff criteria should be used for various properties in a virtual screening. The full list of molecules investigated is provided in Table S3 of the ESI.† The molecules in this family in general have a stable, reversible cyclic voltammetry (CV) signal at low potential (~ 0.1 – 0.2 V), but do not have a reversible peak at high potential (~ 1.0 V). The CVs are provided in Fig. S3–S5 in the ESI.† We focus on alizarin red S (molecule indicated in Fig. S6A†), which was subject to a single charging cycle in a flow cell. At 50% state of charge, an aliquot was taken and separated with high-performance liquid chromatography. The separated components were detected with mass spectrometry (MS), which allowed for assignment of the molecules present at 50% state of charge.

Molecules were detected in two mass channels. The first detected molecule is the starting material (Fig. S6A†) with evidence of a small amount of impurity that corresponds to a sulfonate functionalization at a different position. The second detected mass (Fig. S6B†) has a mass consistent with two products: (1) Michael addition to the fully oxidized form of alizarin red S at the 4 position and subsequent tautomerization or (2) *gem*-diol formation on the fully oxidized form of alizarin red S, which theoretical calculations predict to be most thermodynamically favored at the 1 position (a smaller third peak is also detected, which is most likely the product of one of these processes on the impurity). When the mode of nucleophilic attack is Michael addition, it is effectively a reduction of the system (Fig. 1D) after tautomerization.

The LC-MS results raise the question on the extent of the vulnerability of the fully-oxidized molecule to Michael attack in the presence of water. It is possible to chemically synthesize the oxidized form of quinizarin (Fig. S7 of the ESI†) and leave it in solution overnight. In the presence of H_2SO_4 , the molecule decomposes to some extent, but not completely, which implies that the oxidized form is at least stable on a measurable timescale.

For reference, the PM7 COSMO-calculated Michael addition energy to alizarin red S is 0.03 eV (lower susceptibility than predicted for tiron: 0.25 eV), which we use as an upper cutoff for the virtual screening criteria below.

2.4 Effects of Michael addition on reduction potential

Given the theoretical and experimental evidence for the susceptibility of high reduction potential quinones to Michael addition/substitution, the next important question to address is the ultimate effects of Michael addition on battery performance. To investigate this, we found ~ 1700 molecules in our database that had been generated through combinatorics that are also Michael addition/substitution products of other molecules in our database and evaluated the reduction potential of these Michael products. The effects of Michael addition/substitution on the reduction potential show a bimodal distribution (Fig. 4A). The first of these modes clustered around a -0.15 to -0.2 V shift in reduction potential upon Michael addition. This cluster consists of molecules that maintain the same redox-active topology as before Michael addition and the decrease in the reduction potential simply comes from the increased

electron density on the quinone core, due to the electron-donating tendencies of hydroxyl groups. The second cluster of molecules is centered around a -0.5 V shift in reduction potential. These correspond to molecules where the redox pattern is changed, for instance a 1-2 quinone becomes a 1-4 quinone. In both cases, Michael addition will substantially decrease the OCV of any battery that uses the Michael-susceptible molecule as a posolyte, as has been seen in tiron.⁶ In addition, the first Michael addition product may also be susceptible to further reactions with water; this would further decrease performance. Thus, it is most reasonable to search for molecules lacking thermodynamic susceptibility to Michael addition to begin with.

2.5 Number of promising candidates at all reduction potentials

Fig. 4B shows the number of molecules of particular categories with a Michael addition site that satisfy stability criteria, on a logarithmic scale. The stability criteria that were employed are:

(1) Calculated $\log K_{\text{hyd}} < 1.0$, this corresponds the *gem*-diol form of a molecule being less than 10 times more abundant, in equilibrium, than the oxidized form of the molecule. Although *gem*-diol formation is still more favored when K_{hyd} is between 1 and 10, the redox-active ketone form may be present in sufficient quantity to give satisfactory battery performance.

(2) $\Delta E_{\text{mic}} < 0.03$ eV, this cutoff means that the molecule is less susceptible to Michael addition than alizarin red S, which we showed *via* LC-MS undergoes Michael addition.

At the low reduction potentials (< 0.2 V), hundreds of molecules are calculated to be thermodynamically stable, even though our library was biased towards discovering high-reduction-potential molecules by employing electron withdrawing groups. However, at high reduction potentials (> 0.95 V *vs.* SHE), the number of stable molecules drops off precipitously, especially if exotic phenanthrene-functionalized molecules or oxidized catechols (which may be vulnerable to kelation reactions) are excluded. The surviving molecules are enormously rare, numbering in the tens (and are shown in Fig. S9 and S10,† with estimated solubility computed using ChemAxon,³⁰ in the ESI†). Given that there is a mean absolute error associated with the PM7 COSMO calculations of about 0.07 V for reduction potentials and 1.3 log units for $\log K_{\text{hyd}}$ from our calibrated results, it is possible that the molecules that are passing the stability screening are the molecules with larger calculations errors and thus are false positives. Ideally, the strongest candidates from a virtual screening will pass the screening criteria by several multiples of the error bars associated with the calculations; the absence of said molecules suggests that molecules with the desired properties are especially rare for “traditional” quinones with straightforward modifications. Making the criteria more stringent ($\log K_{\text{hyd}} < 0.0$ and $\Delta E_{\text{mic}} < 0.00$ eV) dramatically reduces the number of viable molecules (Fig. S11†). It should be noted that there is a population of about 40 000 pairs, containing mostly exotic phenanthrene-functionalized quinones, with oxidized forms

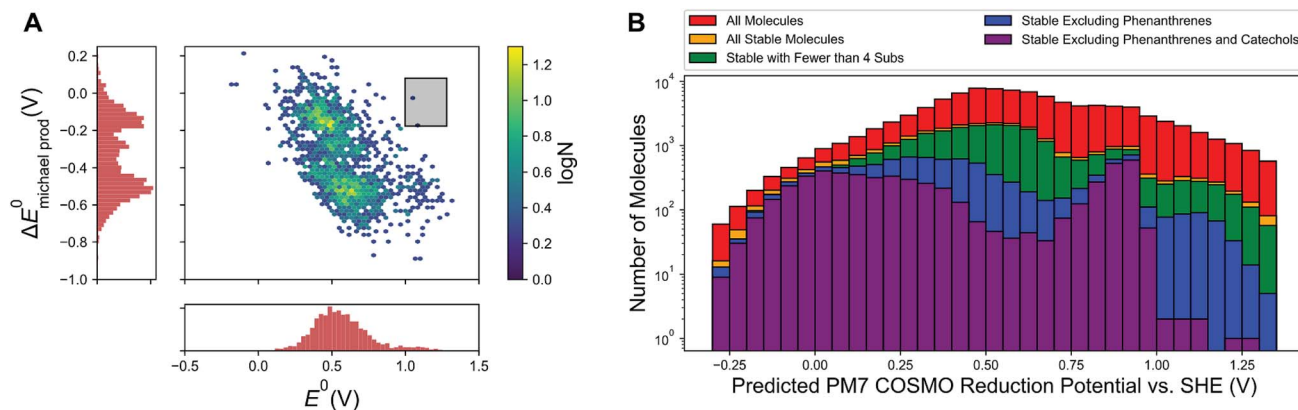


Fig. 4 (A) Change in the reduction potential of a molecule upon Michael addition, 1763 molecules pictured. The desired region, high potential molecules that show almost no change in reduction potential upon Michael addition, is shaded in the black box and contains only two molecules (sulfonated 1–4 benzoquinones), which are shown in Fig. S8.† (B) Plot of the redox potential distributions of various sets of molecules, as indicated in the legend. Molecules are defined as “stable” if they have the following criteria (1) PM7 COSMO Michael addition energy < 0.03 eV and (2) $\log K_{\text{hyd}} < 1.0$.

lacking a valid Michael addition site according to the substitution rules we formulated. These are potentially viable, resulting in about 1500 pairs whose oxidized form has a predicted reduction potential > 0.95 V vs. SHE. A sampling of these is enumerated in Fig. S12 in the ESI† and the full list is provided in a computer-readable format. These molecules are expected to be challenging to synthesize and it is possible that they are subject to other decomposition mechanisms not considered in this work, but they constitute a substantial fraction of the most promising molecules at this juncture.

3 Conclusion

Taking the computational screening and the experimental results together, it is not surprising that the highest reduction potential quinone that has been demonstrated with any full cell cycling in acid reported to date has a reduction potential at 0.85 V vs. SHE (DHDMB).⁸ This lies very close to the stability cliff that we observed in our library, which is between 0.90 and 0.95 V. These results have several implications for the future development of an all-organic redox flow battery. We found almost no quinones that are based on currently used backbones with currently employed functional groups that are both high in reduction potential (leading to > 1.0 V OCV when paired against another quinone) and thermodynamically protected from Michael addition and/or *gem*-diol formation. Going forward, two pathways for exploration that do not involve fused quinones are apparent: (1) attempt to synthesize the exotic phenanthrene-based quinones (which may be susceptible to other not-yet-observed decomposition mechanisms, see Scheme S1 in the ESI† for another potential mechanism), or (2) employ strategies to mitigate the Michael addition from a kinetics perspective. Our calculations indicate that the thermodynamic susceptibility to Michael substitution is about 0.13 eV less than the thermodynamic susceptibility to Michael addition between potentials of 1.00 and 1.05 V after averaging over all of the R-groups considered in this study. This can be taken a step further, by

developing molecules which, while thermodynamically susceptible to Michael addition, may not be kinetically susceptible, through protection with bulky groups. This strategy has the drawback of adding molecular weight and potentially increasing synthetic cost and decreasing the solubility of the molecules. It would also be desirable to screen for this computationally (as opposed to here, where we investigated the highest energy intermediate along the nucleophilic addition pathway), though transition state searches are expensive. While introducing a bulky functional group to block the Michael addition/substitution site makes sense from a kinetics perspective, it is not clear what strategy might be employed to mitigate the effects of *gem*-diol formation. The groups could also lead to the stabilization of tertiary carbocations if the molecule is protonated in acidic solution. The formation of these carbocations was recently reported as a key step in the capacity fade mechanism for DHDMB.³¹ Another potential strategy could be to modulate the pK_{a} s of the redox-active sites of the reduced form of these couples. This would lead to a “flattening out” of the potential on the Pourbaix diagram at lower pH and could lead to otherwise unpromising molecules at pH = 0 becoming viable at higher values of pH. Additionally, it may be necessary to investigate other organic molecule or low-cost metal complex^{9,10} motifs to find molecules that are less susceptible to water attack, while still providing the high reduction potential and energy density. Finally, although aqueous redox flow batteries have large advantages in terms of solvent cost and conductivity over non-aqueous systems, the absence of these water-driven instability mechanisms explored here in the latter makes further research and development intriguing.

4 Experimental methods

Flow cells were constructed similar to previous reports.^{3,18} Pyrosealed POCO graphite flow plates were used for both electrodes. Each electrode comprised a 5 cm² geometric surface

area covered by a stack of three sheets of Sigracet SGL 39AA porous carbon paper pre-baked in air overnight at 400 °C. The membrane used was Nafion 117. The pumping rate was 60 mL min⁻¹. The positive electrolyte used was 7 mL 0.1 M alizarin red S dissolved in 1 M sulfuric acid. The negative electrolyte used was 30 mL 0.2 M 2,7-anthraquinone-disulfonic acid dissolved in 1 M sulfuric acid. Aliquots were taken out at 50% state-of-charge in the first charging cycle as calculated by coulometry.

High-resolution LC-MS analysis of alizarin red S decomposition products was performed in the Small Molecule Mass Spectrometry Facility at Harvard on a Bruker Impact II q-TOF with internal calibration by sodium formate clusters. Liquid chromatography was performed on an Agilent 1290 Infinity HPLC using a Allure PFPP column (5 μm particle size, 150 × 2.1 mm) at a flow rate of 0.4 mL min⁻¹ and the following elution conditions were applied (solvent A = 0.1% v/v formic acid in water; solvent B = 0.1% v/v formic acid in acetonitrile): 100% solvent A for 2 min, a gradient increasing from 0% to 15% solvent B in solvent A over 13 min, a gradient increasing to 100% solvent B over 5 min, a gradient decreasing to 0% solvent B in solvent A over 0.1 min, and 100% solvent A for 4.9 min. The ESI mass spectra were recorded in negative ionization mode.

5 Computational methods

5.1 Library generation

Molecular libraries were generated programmatically, using several aromatic backbones (benzene, naphthalene, and anthracene from a previous study²⁶ and phenanthrene and tetracene, which are new for this work; see Fig. 1) using the open-source cheminformatics suite RDKit.³² The previous study²⁶ showed that the two-proton, two-electron redox processes in benzo-, naphtho-, and anthraquinones can be modulated by changing the number and position of various substituents along with the positions of the redox-active ketones. The results from that work, using single and full substitution patterns, match organic chemistry principles. This suggests that electron-donating groups (EDG) such as -OH and electron-withdrawing groups (EWG) such as -COOH, -SO₃H, -PO₃H₂ can tune E_0 while maintaining high aqueous solubility and synthetic accessibility.

For this work, molecules were generated using all possible substitution patterns for each of the three electron withdrawing groups alone and in combination with hydroxyls. In addition, the quinone dataset was expanded *via* intuition-driven suggestions from experimental collaborators. The molecules generated were used as the reduced parts of redox pairs and subject to two-proton, two-electron oxidation reactions. The R-groups that were included for all backbones were carboxylic, hydroxyl, phosphonic, and sulfonic. In addition, for benzoquinones methylimidazolium, methylpyridinium, and tetramethylimidazolium groups were included on benzoquinones based on feedback from experimentalists.

The presence of multiple hydroxyl R-groups implies multiple oxidation patterns for a given molecule, but only one isomer will be thermodynamically predominant at virtually any given redox potential. Redox pairs were stored in a database as objects with

pointers to reduced and oxidized molecules, allowing us to build reactivity graphs. The ability to create and track molecular linkages allowed us to book-keep the relationships between the species and to calculate pairwise properties, such as reaction free energies.

The presence of multiple substitutions also expands the idea of blocking of Michael addition. This blockage was less likely to happen in the previous one-substitution studies. However, these substituents are also good leaving groups, so the important quantity to examine is the relative energy of the tetrahedral intermediate of the Michael substitution. If this step in the proposed mechanism is thermodynamically favored, then we assume that substitution is favored overall.

Whereas some of the patterns may appear rare and are thermodynamically unfavorable if alternative oxidations exist, it is important to include them. Otherwise a fraction of the molecules in a reaction graph could be outside the library, and thus completely ignored. In total, 146 857 quinone/hydroquinone pairs were generated. Corresponding *gem*-diols for each oxidized molecule were also included in the database. We also included decomposition products associated with irreversible Michael addition of water onto α - β unsaturated carbonyls (or α - γ , α - δ , *etc.* when available). Depending on the substitution of the β site, two potential pathways are possible:

(1) For hydrogen-substituted sites, this reaction results in an intermediate enol, which isomerizes to a reduced, hydroxylated hydroquinone (Fig. 1C). Thus, the final product of this reaction is an electrochemically active quinone, although it is in the reduced state, so it needs to be oxidized again to recover the stored charge. However, this molecule can have significantly different electrochemical behavior than the original electrolyte with a much lower potential.

(2) For functionalized β sites and depending on the nature of the substituent, the addition can be followed by loss of the R-group and isomerization to hydroquinone. Bulky substituents will have a significant steric effect, increasing the barrier for water addition.

98 043 Michael addition products were generated from these pairs, based on the allowed patterns considered above. Both Michael substitution and Michael addition were allowed. We originally explored other avenues for exploring reactivity. Fukui functions³³ are known to be good qualitative descriptors for broad classes of reactivity,³⁴ but for our application here where we seek a quantitative assessment of known, well-defined mechanisms, direct computation of the landscape of products and intermediates is more appropriate.^{35,36}

5.2 Electronic structure methods

Quantum chemistry is the bottleneck of this virtual screening study. In the previous study on a select group of singly and fully-substituted quinones (totaling 1710 quinone molecules), plane wave DFT calculations were employed.²⁶ Here, on a molecular screening study with ~1 000 000 molecules (considering all of the potential decomposition products that are also considered), lower cost electronic structure methods are needed that also maintain accuracy similar to the previous study. Other recent

studies have also demonstrated capability of different levels of DFT (with and without calibration and/or explicit solvation) to estimate the reduction potentials of organic molecules, including quinones.^{4,27,37,38}

The calculated reaction energies for both reduction and *gem*-diol reactions were benchmarked against experimental reduction potentials and *gem*-diol hydration equilibrium constants (Tables S1 and S2 of the ESI†) at several different levels of electronic structure theory. Benchmarking studies have been performed at the following levels of theory: PBE/6-31G(d) optimization and B3LYP/6-31G(d) optimization, B3LYP/6-311+G(d,p) gas-phase single point (at PBE/6-31G(d) gas-phase geometries), and B3LYP/6-311+G(d,p) PCM single point energies using the CPCM as implemented in QChem 4.0 with water as the solvent.³⁹ The PBE/6-31G(d) optimizations were implemented using TeraChem.^{40,41} Semi-empirical methods were also benchmarked; the energies were computed at both the PM7 and PM7 with the COSMO solvation model with water as a solvent (referred to as PM7 and PM7 COSMO, respectively).

We have performed a benchmark study of these cheaper methods and compared their ability to predict the reduction potential and hydration equilibrium constant.

Using a well-characterized experimental set of reduction potential measurements, we tested the calibration scheme by comparing the zero-temperature reaction electronic energy for the reduction (E_{red}) with experimentally-determined quinone reduction potentials (E^0) in aqueous solution (pH = 0) at 298 K.²⁶ Notwithstanding computational affordability, all the methods are close in the accuracy of their predictions (see ESI Fig. S1†).

Similarly, we carried out a calibration of the hydration equilibrium constant by mapping zero-temperature energy differences for the carbonyl hydration reaction (E_{hyd}) with experimentally determined equilibrium constants⁴² (K_{hyd}) in water at 298 K.

When considering both the accuracy and computational cost of the various methods, the PM7 COSMO optimization has the best balance. B3LYP/6-311+G(d,p) (PCM) gives a marginally lower deviation on the calibration set, but does not justify the extra cost here.

As stated above, for computing the vulnerability to Michael addition/substitution, we did not have a body of data against which to calibrate. However, we can use the results of tiron and alizarin red S to gain a sense of scale. At the PM7 COSMO level of theory, the Michael addition free energy for water addition to tiron is 0.25 eV and that of alizarin red S is 0.03 eV. We expect the K_{hyd} and Michael addition energy calculations to be of the most utility in acidic and neutral pH—the regime where water (and not hydroxide) is the primary nucleophilic species present.

Conflicts of interest

L. T., R. G. G., M. J. A., and A. A.-G. are inventors on a patent application “Quinone and Hydroquinone Based Flow Battery.” Patent Application US20160248114A1. Filed by Harvard University.

Acknowledgements

Research at Harvard was supported by the Innovation Fund Denmark *via* the Grand Solutions project “ORBATS” file nr. 7046-00018B, U.S. DOE ARPA-E award DE-AR0000767, and the Massachusetts Clean Energy Technology Center. This work was also supported by the National Science Foundation through grant No. CBET-1509041. A. A.-G. is very thankful to the Canadian Institute for Advanced Research (CIFAR) for their generous support and collaborations. A. A.-G. thanks Anders G. Frøseth for the generous support of his work. A. A.-G. acknowledges support from the Canada 150 Research Chairs Program.

References

- 1 F. R. Brushett, J. T. Vaughey and A. N. Jansen, *Adv. Energy Mater.*, 2012, **2**, 1390–1396.
- 2 B. Huskinson, M. P. Marshak, C. Suh, S. Er, M. R. Gerhardt, C. J. Galvin, X. Chen, A. Aspuru-Guzik, R. G. Gordon and M. J. Aziz, *Nature*, 2014, **505**, 195–198.
- 3 K. Lin, Q. Chen, M. R. Gerhardt, L. Tong, S. B. Kim, L. Eisenach, A. W. Valle, D. Hardee, R. G. Gordon, M. J. Aziz and M. P. Marshak, *Science*, 2015, **349**, 1529–1532.
- 4 K. Lin, R. Gómez-Bombarelli, E. S. Beh, L. Tong, Q. Chen, A. Valle, A. Aspuru-Guzik, M. J. Aziz and R. G. Gordon, *Nat. Energy*, 2016, **1**, 16102.
- 5 T. Liu, X. Wei, Z. Nie, V. Sprenkle and W. Wang, *Adv. Energy Mater.*, 2016, **6**, 1501449.
- 6 B. Yang, L. Hooper-Burkhardt, F. Wang, G. K. S. Prakash and S. R. Narayanan, *J. Electrochem. Soc.*, 2014, **161**, A1371–A1380.
- 7 T. Janoschka, N. Martin, M. D. Hager and U. S. Schubert, *Angew. Chem., Int. Ed.*, 2016, **55**, 14427–14430.
- 8 L. Hooper-Burkhardt, S. Krishnamoorthy, B. Yang, A. Murali, A. Nirmalchandar, G. K. S. Prakash and S. R. Narayanan, *J. Electrochem. Soc.*, 2017, **164**, A600–A607.
- 9 B. Hu, C. DeBruiler, Z. Rhodes and T. L. Liu, *J. Am. Chem. Soc.*, 2017, **139**, 1207–1214.
- 10 E. S. Beh, D. De Porcellinis, R. L. Gracia, K. T. Xia, R. G. Gordon and M. J. Aziz, *ACS Energy Lett.*, 2017, **2**, 639–644.
- 11 J. A. Kowalski, M. D. Casselman, A. P. Kaur, J. D. Milshtein, C. F. Elliott, S. Modekrutti, N. H. Attanayake, N. Zhang, S. R. Parkin, C. Risko, F. R. Brushett and S. A. Odom, *J. Mater. Chem. A*, 2017, **5**, 24371–24379.
- 12 W. Duan, J. Huang, J. A. Kowalski, I. A. Shkrob, M. Vijayakumar, E. Walter, B. Pan, Z. Yang, J. D. Milshtein, B. Li, C. Liao, Z. Zhang, W. Wang, J. Liu, J. S. Moore, F. R. Brushett, L. Zhang and X. Wei, *ACS Energy Lett.*, 2017, **2**, 1156–1161.
- 13 T. Quan, R. D. Milton, S. Abdellaoui and S. D. Minter, *Chem. Commun.*, 2017, **53**, 8411–8414.
- 14 C. S. Sevov, K. H. Hendriks and M. S. Sanford, *J. Phys. Chem. C*, 2017, **121**, 24376–24380.
- 15 Z. Yang, L. Tong, D. P. Tabor, E. S. Beh, M.-A. Goulet, D. De Porcellinis, A. Aspuru-Guzik, R. G. Gordon and M. J. Aziz, *Adv. Energy Mater.*, 2018, **8**, 1702056.

- 16 G. Kwon, S. Lee, J. Hwang, H.-S. Shim, B. Lee, M. H. Lee, Y. Ko, S.-K. Jung, K. Ku, J. Hong and K. Kang, *Joule*, 2018, **2**, 1771–1782.
- 17 A. Hollas, X. Wei, V. Murugesan, Z. Nie, B. Li, D. Reed, J. Liu, V. Sprenkle and W. Wang, *Nat. Energy*, 2018, **3**, 508–514.
- 18 D. G. Kwabi, K. Lin, Y. Ji, E. F. Kerr, M.-A. Goulet, D. De Porcellinis, D. P. Tabor, D. A. Pollack, A. Aspuru-Guzik, R. G. Gordon and M. J. Aziz, *Joule*, 2018, **2**, 1894–1906.
- 19 Y. Ji, M.-A. Goulet, D. A. Pollack, D. G. Kwabi, S. Jin, D. De Porcellinis, E. F. Kerr, R. G. Gordon and M. J. Aziz, *Adv. Energy Mater.*, 2019, 1900039.
- 20 K. Wedege, E. Dražević, D. Konya and A. Bentien, *Sci. Rep.*, 2016, **6**, 39101.
- 21 J. Carretero-Gonzalez, E. Castillo-Martinez and M. Armand, *Energy Environ. Sci.*, 2016, **9**, 3521–3530.
- 22 B. Huskinson, M. Marshak, M. J. Aziz, R. G. Gordon, A. Aspuru-Guzik, S. Er, C. Suh, L. Tong and K. Lin, Quinone and Hydroquinone Based Flow Battery, Patent Application US20160248114A1, 2016.
- 23 A. E. Wendlandt and S. S. Stahl, in *Quinones in Hydrogen Peroxide Synthesis and Catalytic Aerobic Oxidation Reactions*, John Wiley & Sons, Ltd, 2016, ch. 14, pp. 219–237.
- 24 M. R. Gerhardt, L. Tong, R. Gómez-Bombarelli, Q. Chen, M. P. Marshak, C. J. Galvin, A. Aspuru-Guzik, R. G. Gordon and M. J. Aziz, *Adv. Energy Mater.*, 2017, **7**, 1601488.
- 25 M.-A. Goulet, L. Tong, D. A. Pollack, D. P. Tabor, S. A. Odom, A. Aspuru-Guzik, E. E. Kwan, R. G. Gordon and M. J. Aziz, *J. Am. Chem. Soc.*, 2019, DOI: 10.1021/jacs.8b13295.
- 26 S. Er, C. Suh, M. P. Marshak and A. Aspuru-Guzik, *Chem. Sci.*, 2015, **6**, 885–893.
- 27 S. D. Pineda Flores, G. C. Martin-Noble, R. L. Phillips and J. Schrier, *J. Phys. Chem. C*, 2015, **119**, 21800–21809.
- 28 James J. P. Stewart, *MOPAC2016, Stewart Computational Chemistry*, Colorado Springs, CO, USA, 2016, <http://OpenMOPAC.net>.
- 29 A. Klamt and G. Schuurmann, *J. Chem. Soc., Perkin Trans. 2*, 1993, 799–805.
- 30 *Marvin 18.1.0*, 2018, ChemAxon, <http://www.chemaxon.com>.
- 31 A. Murali, A. Nirmalchandar, S. Krishnamoorthy, L. Hooper-Burkhardt, B. Yang, G. Soloveichik, G. K. S. Prakash and S. R. Narayanan, *J. Electrochem. Soc.*, 2018, **165**, A1193–A1203.
- 32 G. Landrum, *RDKit: Open-source cheminformatics*, <http://www.rdkit.org>.
- 33 Y. Li and J. N. S. Evans, *J. Am. Chem. Soc.*, 1995, **117**, 7756–7759.
- 34 L. R. Domingo, M. Ríos-Gutiérrez and P. Pérez, *Molecules*, 2016, 748.
- 35 F. Méndez and J. L. Gázquez, *J. Am. Chem. Soc.*, 1994, **116**, 9298–9301.
- 36 J. L. Gázquez and F. Méndez, *J. Phys. Chem.*, 1994, **98**, 4591–4593.
- 37 M. T. Huynh, C. W. Anson, A. C. Cavell, S. S. Stahl and S. Hammes-Schiffer, *J. Am. Chem. Soc.*, 2016, **138**, 15903–15910.
- 38 H. Kim, T. Goodson and P. M. Zimmerman, *J. Phys. Chem. C*, 2016, **120**, 22235–22247.
- 39 Y. Shao, Z. Gan, E. Epifanovsky, A. T. Gilbert, M. Wormit, J. Kussmann, A. W. Lange, A. Behn, J. Deng, X. Feng, D. Ghosh, M. Goldey, P. R. Horn, L. D. Jacobson, I. Kaliman, R. Z. Khaliullin, T. Kuś, A. Landau, J. Liu, E. I. Proynov, Y. M. Rhee, R. M. Richard, M. A. Rohrdanz, R. P. Steele, E. J. Sundstrom, H. L. Woodcock III, P. M. Zimmerman, D. Zuev, B. Albrecht, E. Alguire, B. Austin, G. J. O. Beran, Y. A. Bernard, E. Berquist, K. Brandhorst, K. B. Bravaya, S. T. Brown, D. Casanova, C.-M. Chang, Y. Chen, S. H. Chien, K. D. Closser, D. L. Crittenden, M. Diedenhofen, R. A. DiStasio Jr, H. Do, A. D. Dutoi, R. G. Edgar, S. Fatehi, L. Fusti-Molnar, A. Ghysels, A. Golubeva-Zadorozhnaya, J. Gomes, M. W. Hanson-Heine, P. H. Harbach, A. W. Hauser, E. G. Hohenstein, Z. C. Holden, T.-C. Jagau, H. Ji, B. Kaduk, K. Khistyayev, J. Kim, J. Kim, R. A. King, P. Klunzinger, D. Kosenkov, T. Kowalczyk, C. M. Krauter, K. U. Lao, A. D. Laurent, K. V. Lawler, S. V. Levchenko, C. Y. Lin, F. Liu, E. Livshits, R. C. Lochan, A. Luenser, P. Manohar, S. F. Manzer, S.-P. Mao, N. Mardirossian, A. V. Marenich, S. A. Maurer, N. J. Mayhall, E. Neuscamman, C. M. Oana, R. Olivares-Amaya, D. P. O'Neill, J. A. Parkhill, T. M. Perrine, R. Peverati, A. Prociuk, D. R. Rehn, E. Rosta, N. J. Russ, S. M. Sharada, S. Sharma, D. W. Small, A. Sodt, T. Stein, D. Stück, Y.-C. Su, A. J. Thom, T. Tsuchimochi, V. Vanovschi, L. Vogt, O. Vydrov, T. Wang, M. A. Watson, J. Wenzel, A. White, C. F. Williams, J. Yang, S. Yeganeh, S. R. Yost, Z.-Q. You, I. Y. Zhang, X. Zhang, Y. Zhao, B. R. Brooks, G. K. Chan, D. M. Chipman, C. J. Cramer, W. A. Goddard III, M. S. Gordon, W. J. Hehre, A. Klamt, H. F. Schaefer III, M. W. Schmidt, C. D. Sherrill, D. G. Truhlar, A. Warshel, X. Xu, A. Aspuru-Guzik, R. Baer, A. T. Bell, N. A. Besley, J.-D. Chai, A. Dreuw, B. D. Dunietz, T. R. Furlani, S. R. Gwaltney, C.-P. Hsu, Y. Jung, J. Kong, D. S. Lambrecht, W. Liang, C. Ochsenfeld, V. A. Rassolov, L. V. Slipchenko, J. E. Subotnik, T. V. Voorhis, J. M. Herbert, A. I. Krylov, P. M. Gill and M. Head-Gordon, *Mol. Phys.*, 2015, **113**, 184–215.
- 40 *TeraChem v 1.9*, PetaChem, LLC, 2009, 2015, see <http://www.petachem.com>.
- 41 I. S. Ufimtsev and T. J. Martinez, *J. Chem. Theory Comput.*, 2009, **5**, 2619–2628.
- 42 R. Gómez-Bombarelli, M. González-Pérez, M. T. Pérez-Prior, E. Calle and J. Casado, *J. Phys. Chem. A*, 2009, **113**, 11423–11428.

Electronic Supplementary Information for “Mapping the Frontiers of Quinone Stability in Aqueous Media: Implications for Organic Aqueous Redox Flow Batteries”

Daniel P. Tabor^{#,†}, Rafael Gómez-Bombarelli^{#,†,‡}, Liuchuan Tong,[†] Roy G.
Gordon,^{†,¶} Michael J. Aziz,[¶] and Alán Aspuru-Guzik^{*,†,§,||}

[†]*Department of Chemistry and Chemical Biology, Harvard University, Cambridge, MA
02138 USA*

[‡]*Present Address: Department of Materials Science and Engineering, Massachusetts
Institute of Technology, Cambridge, MA 02139 USA*

[¶]*Harvard John A. Paulson School of Engineering and Applied Sciences, Cambridge,
Massachusetts 02138 USA*

[§]*Department of Chemistry and Department of Computer Science, University of Toronto,
Toronto, Ontario M5S 3H6, Canada*

^{||}*Vector Institute, Toronto, ON M5G 1M1, Canada.*

E-mail: alan@aspuru.com

[#] These authors contributed equally to this work.

Contents

S1 Calibration of Reduction Potentials with PM7 and B3LYP Methods S3

S2 Experimental Calibration Points for Theoretical Methods	S4
S3 Summary of Experimental Stability Results	S6
S4 Chemical Synthesis of Oxidized Quinizarin	S12
S5 Molecules with Small Changes in Redox Properties Upon Michael Addition	S13
S6 Molecules that Pass Screening Criteria	S14
S7 Potential Ring Opening Decomposition Mechanism	S18
References	S18

S1 Calibration of Reduction Potentials with PM7 and B3LYP Methods

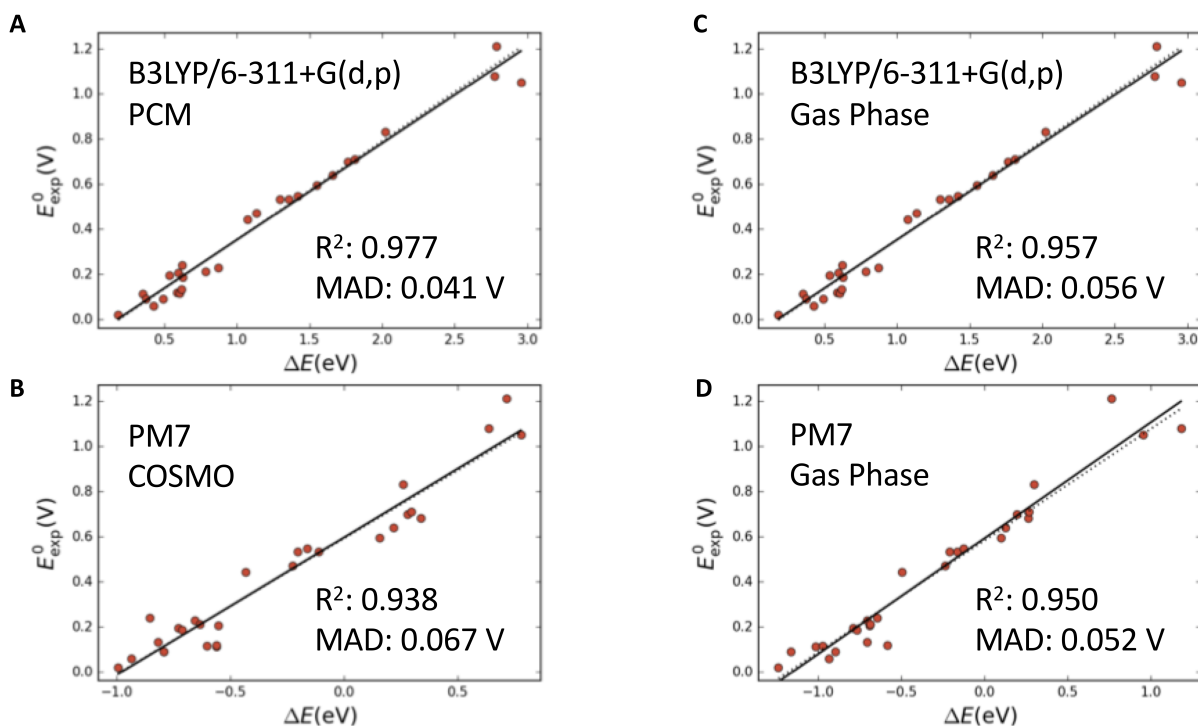


Figure S1: Calibration of the computed reduction potentials of quinones with PM7 COSMO and B3LYP/6-311+G(d,p) PCM methods. ΔE refers to the calculated reaction energy of oxidized form and H_2 combining to form the reduced hydroquinone at the given level of theory and E_{exp}^0 refers to the measured reduction potential at pH = 0 vs. SHE. The values of the previously measured standard reduction potentials and the identities of the molecules are tabulated in Table S1.

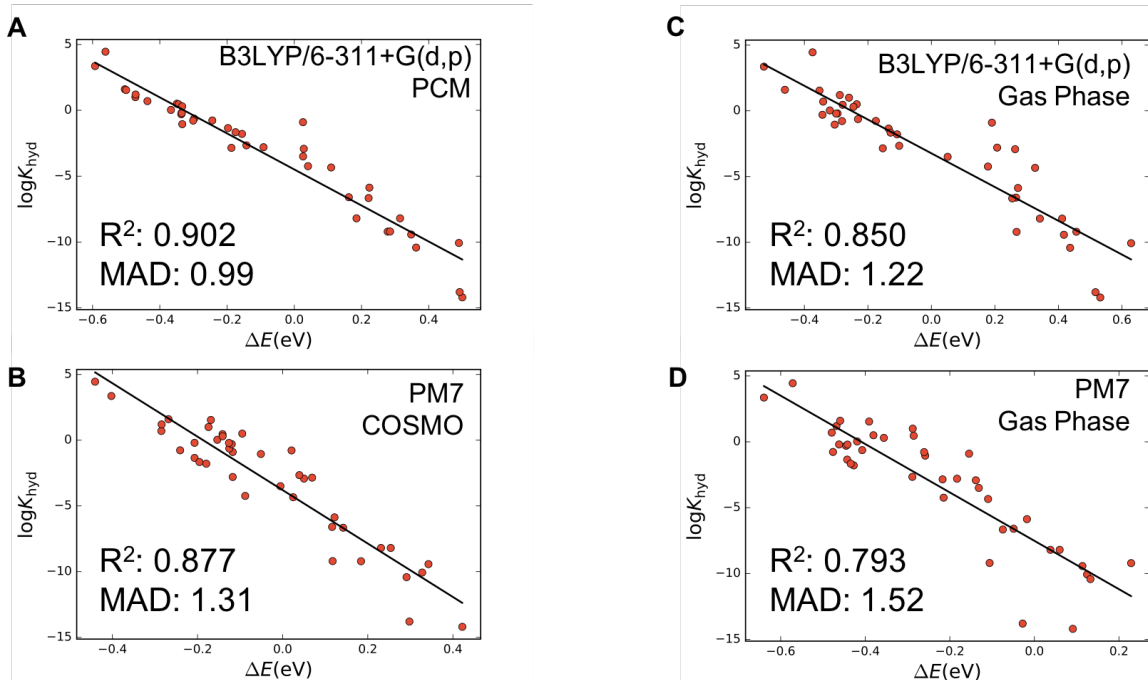


Figure S2: Calibration of the gem diol equilibrium constant, $\log K_{\text{hyd}}$, with PM7 COSMO and B3LYP/6-311+G(d,p) PCM methods. ΔE refers to the calculated reaction energy of a ketone and water combining to form a gem diol at the given level of theory. and E_{exp}^0 The values of the previously measured standard reduction potentials and the identities of the molecules are tabulated in Table S2. These results were first reported in Ref. S1

S2 Experimental Calibration Points for Theoretical Methods

Note: In the case of multiple ketone groups (as is the case with all quinones), the reported $\log K_{\text{hyd}}$ is for the most thermodynamically favorable reaction for the formation of a gem diol.

Table S1: Reference Data for Calibration of Reduction Potentials

Molecule SMILES	E_{exp}^0 vs. SHE (V) at pH = 0
<chem>Oc1c(Cl)c(Cl)c(O)c(Cl)c1Cl</chem>	0.683
<chem>O=S(=O)(O)Cc1c(CS(=O)(=O)O)c(O)c2c(O)c3ccccc3c(O)c2c1O</chem>	0.02
<chem>O=S(=O)(O)CCSc1c(SCCS(=O)(=O)O)c(O)c2c(O)c3ccccc3c(O)c2c1O</chem>	0.113
<chem>O=S(=O)(O)c1cc(O)c2c(O)c3ccccc3c(O)c2c1O</chem>	0.09
<chem>O=S(=O)(O)c1cc2c(O)c3ccccc3c(O)c2c(O)c1O</chem>	0.06
<chem>Oc1c2ccccc2c(O)c2ccccc12</chem>	0.09
<chem>O=S(=O)(O)c1cccc2c(O)c3ccccc3c(O)c12</chem>	0.195
<chem>O=S(=O)(O)c1ccc2c(O)c3ccc(S(=O)(=O)O)c(O)c3c(O)c2c1O</chem>	0.118
<chem>O=S(=O)(O)c1cccc2c(O)c3cccc(S(=O)(=O)O)c3c(O)c12</chem>	0.206
<chem>O=S(=O)(O)c1ccc2c(O)c3c(O)c(S(=O)(=O)O)ccc3c(O)c2c1O</chem>	0.116
<chem>O=S(=O)(O)c1ccc2c(O)c3c(O)c(O)c(S(=O)(=O)O)cc3c(O)c2c1</chem>	0.133
<chem>O=S(=O)(O)c1cccc2c(O)c3c(S(=O)(=O)O)cccc3c(O)c12</chem>	0.239
<chem>O=S(=O)(O)c1ccc2c(O)c3ccccc3c(O)c2c1</chem>	0.187
<chem>O=S(=O)(O)c1ccc2c(O)c3ccc(S(=O)(=O)O)cc3c(O)c2c1</chem>	0.213
<chem>O=S(=O)(O)c1ccc2c(O)c3cc(S(=O)(=O)O)ccc3c(O)c2c1</chem>	0.228
<chem>Oc1c(O)c2ccccc2c2ccccc12</chem>	0.442
<chem>Oc1ccc(O)c2ccccc12</chem>	0.47
<chem>O=S(=O)(O)c1cccc2c(O)ccc(O)c12</chem>	0.532
<chem>O=S(=O)(O)c1ccc2c(O)ccc(O)c2c1</chem>	0.534
<chem>Oc1ccc2ccccc2c1O</chem>	0.547
<chem>Oc1ccc(O)c(O)c1</chem>	0.594
<chem>Cc1cc(O)ccc1O</chem>	0.641
<chem>Oc1ccc(O)cc1</chem>	0.699
<chem>Oc1ccc(O)c(Cl)c1</chem>	0.71
<chem>Oc1ccccc1O</chem>	0.831
<chem>O=C1c2ccccc2C(=O)c2c(O)c(SCCS(=O)(=O)O)c(SCCS(=O)(=O)O)c(O)c21</chem>	1.08
<chem>O=C1c2ccccc2C(=O)c2c1cc(S(=O)(=O)O)c(O)c2O</chem>	1.21
<chem>O=C1c2ccccc2C(=O)c2c(O)c(S(=O)(=O)O)cc(O)c21</chem>	1.05

Experimental reduction potentials obtained from Ref. S2.

Table S2: Reference Data for Calibration of $\log K_{\text{hyd}}$

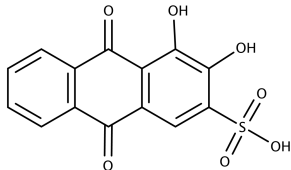
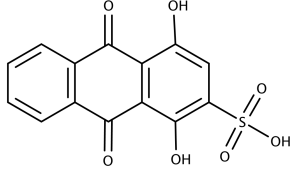
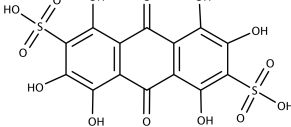
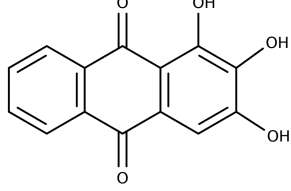
Molecule SMILES	$\log K_{\text{hyd}}$	Molecule SMILES	$\log K_{\text{hyd}}$
<chem>COC(=O)C(F)F</chem>	-2.92	<chem>CC(C)=O</chem>	-2.85
<chem>CCC(=O)OC</chem>	-9.43	<chem>CCCC=O</chem>	-0.3
<chem>O=C1CCC1</chem>	-2.66	<chem>O=CCCl</chem>	1.6
<chem>O=C(CCl)CCl</chem>	1.0	<chem>O=Cc1ccc(Cl)c(Cl)c1</chem>	-1.35
<chem>C=O</chem>	3.36	<chem>COC(=O)c1ccccc1</chem>	-10.07
<chem>COC(=O)C(Cl)(Cl)Cl</chem>	-4.24	<chem>CC(=O)CF</chem>	-0.78
<chem>COC(=O)C(F)(F)F</chem>	-0.9	<chem>CCSC(C)=O</chem>	-8.2
<chem>CCSC(=O)C(F)(F)F</chem>	-2.8	<chem>COC(=O)C(Cl)Cl</chem>	-4.34
<chem>COC=O</chem>	-6.6	<chem>COC(=O)CC#N</chem>	-5.87
<chem>CC=O</chem>	0.03	<chem>O=Cc1ccc(Cl)cc1</chem>	-1.79
<chem>CC(=O)N(C)C</chem>	-14.2	<chem>COC(=O)CCl</chem>	-6.66
<chem>COCC(=O)OC</chem>	-9.21	<chem>O=Cc1ccc([N+](=O)[O-])cc1</chem>	-0.77
<chem>COC(C)=O</chem>	-8.2	<chem>CC(=O)C(F)(F)F</chem>	1.54
<chem>CC(=O)CCl</chem>	-1.05	<chem>COC(=O)C(C)=O</chem>	0.5
<chem>CC(C)(Cl)C=O</chem>	0.7	<chem>O=Cc1cccc(Cl)c1</chem>	-1.66
<chem>CCC=O</chem>	-0.2	<chem>O=Cc1ccccc1</chem>	-2.1
<chem>CCC(Br)C=O</chem>	0.6	<chem>CN(C)C(=O)C(F)(F)F</chem>	-9.2
<chem>CCC(Br)(Br)C=O</chem>	1	<chem>CC(=O)C(Cl)Cl</chem>	0.46
<chem>CCC(Cl)C=O</chem>	1.2	<chem>CC(C)C=O</chem>	-0.21
<chem>CC(C)(C)C=O</chem>	-0.63	<chem>CCSC=O</chem>	-3.5
<chem>CN(C)C=O</chem>	-13.8	<chem>COC(=O)C(C)C</chem>	-10.42
<chem>O=CC(Cl)(Cl)Cl</chem>	4.45	<chem>CC(=O)C(C)=O</chem>	0.3

Experimental hydration equilibrium constants obtained from Ref. S3.

S3 Summary of Experimental Stability Results

Cyclic voltammetry results were obtained under the following conditions: 5-10 mM concentration of the molecule in 1M H_2SO_4 . Scanning rate is 100 mV/s. The working electrode is a glassy carbon electrode. The counter electrode is a platinum wire and the reference electrode is Ag/AgCl. Potentials are vs. SHE and the third CV cycle is plotted.

Table S3: Theoretical Predictions of Experimentally-Tested Fused Quinones

Molecule Name	Structure (Reduced Form)	$\log K_{\text{hyd}}^a$	$\Delta E_{\text{mic}}(\text{eV})^a$
Alizarin red S		0.63	0.03
Quinizarin 2-sulfonic acid		0.43	0.37
Alizarin blue 2B		5.53	0.42
Anthracene brown		2.82	<i>b</i>

^a Calculated with PM7 COSMO for oxidized form

^b No Michael addition/substitution site according to formulated rules.

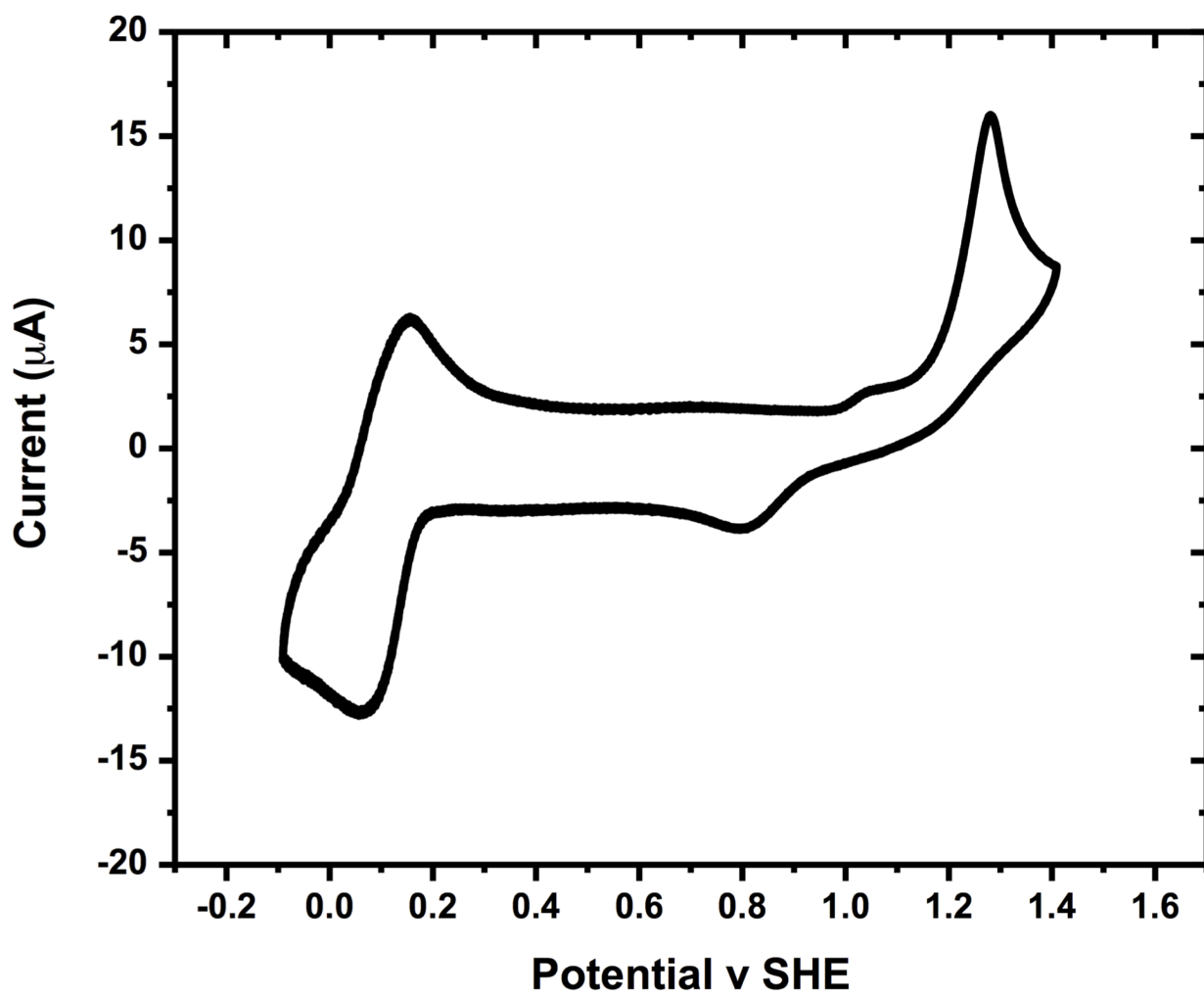


Figure S3: CV of quinizarin 2-sulfonic acid

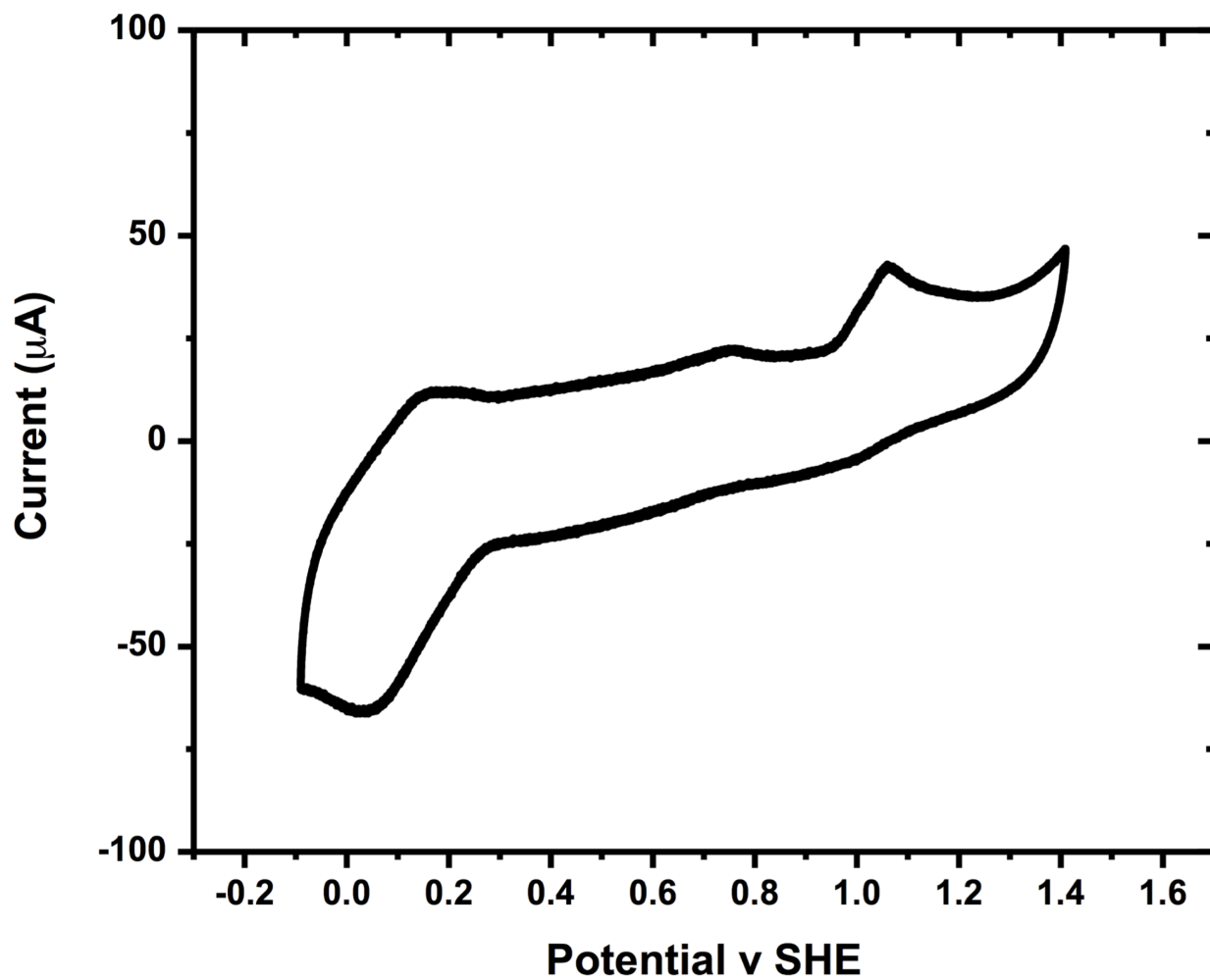


Figure S4: CV of alizarin blue 2B

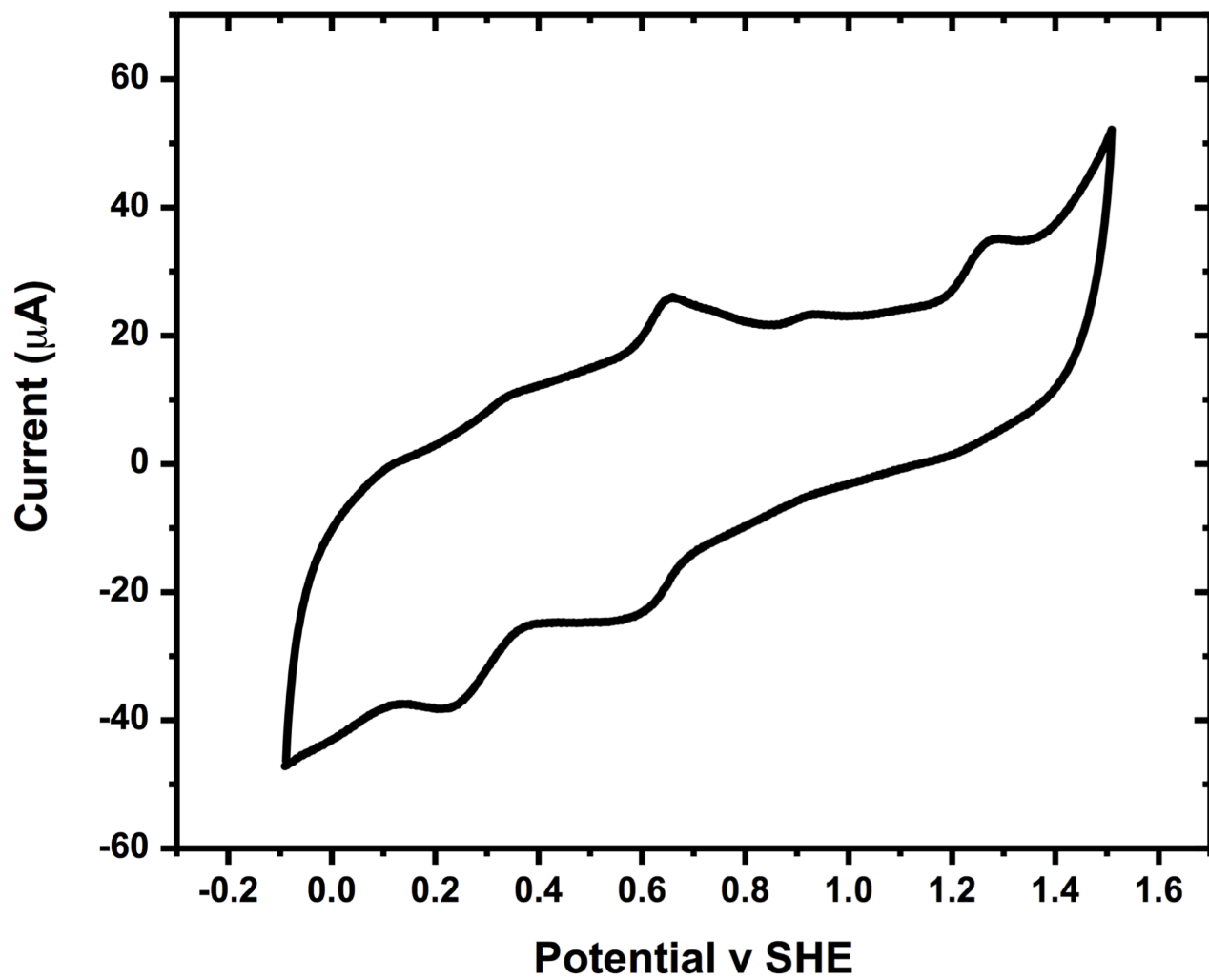


Figure S5: CV of anthracene brown

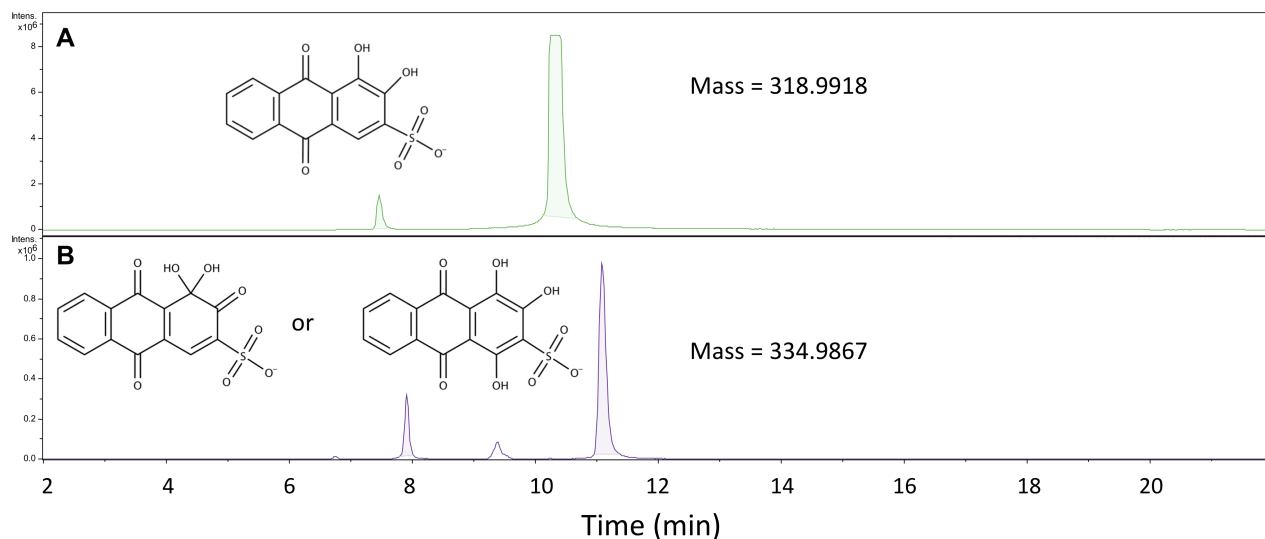


Figure S6: A) LC-MS Spectrum corresponding to starting material, alizarin red S. The two peaks are assigned to different substitution sites of the sulfonate group obtained from the manufacturer, with the dominant material being the depicted structure and the impurity having a sulfonate functionalization at the 7 or 8 position. B) LC-MS spectrum corresponding to the starting material with an additional H_2O mass (after charging). Based on the relative ratios of the starting material to impurities, the peaks at 8 min and 11 min most likely correspond to the Michael addition and gem-diol products of alizarin red S and the much smaller peaks correspond to analogous product(s) in the impurity.

S4 Chemical Synthesis of Oxidized Quinizarin

The oxidized form of quinizarin was chemically synthesized according to literature preparation (Figure S7A).^{S4} The fact that the oxidized quinizarin can be synthesized meant that the molecule itself was accessible. However, by stirring in 1 M sulfuric acid, a solvent often used for flow battery applications, 20 % of the quinizarin was attacked by water and turned into purpurin (Figure S7B). It is worth noting that the solubility of oxidized quinizarin in sulfuric acid was very limited, and in the above model water addition was a heterogeneous reaction. It is conceivable that in a real flow battery setting when a sulfonated fused quinone is employed, the rate of water attack will be orders of magnitude faster.

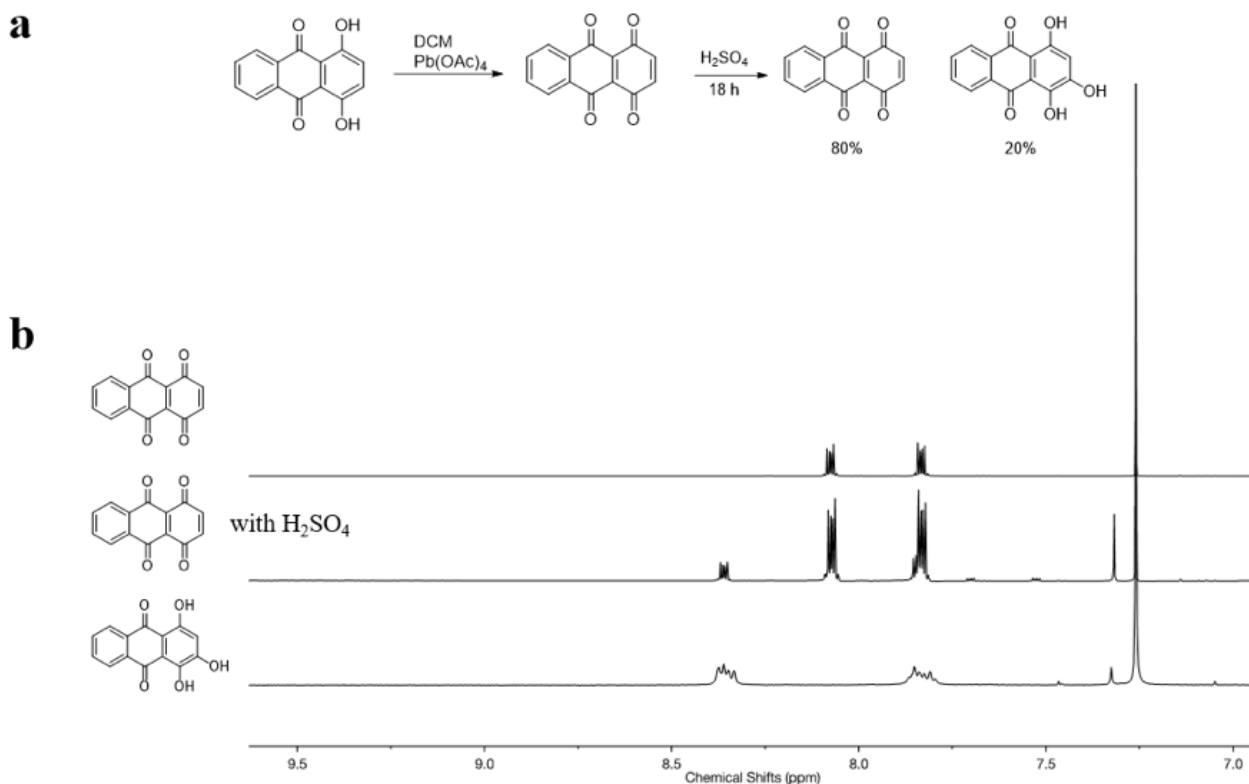


Figure S7: a) Synthesis of oxidized quinizarin. b) NMR spectra of synthetic oxidized quinizarin(top), quinizarin stirred with sulfuric acid (middle), purpurin standard (bottom). NMR spectra were recorded on Varian INOVA 500 spectrometers in solutions of deuterated chloroform (CDCl₃)

S5 Molecules with Small Changes in Redox Properties Upon Michael Addition

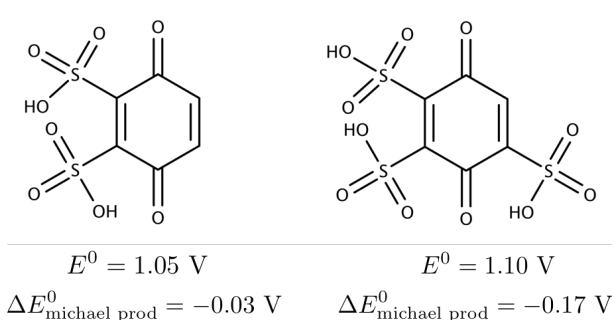


Figure S8: Two molecules (from Figure 3) that are calculated to have reduction potentials $> 1.00 \text{ V}$ vs. SHE at $\text{pH} = 0$ and have Michael addition products that have a change in reduction potential from the parent molecule of less than 0.20 V . Note that the products of Michael addition of these molecules are also subject to a second Michael addition and the reduction potential further decreases. The reduction potential of the dihydroxy, disulfonic acid substituted quinones is calculated to be $\sim 0.80 \text{ V}$ vs. SHE.

S6 Molecules that Pass Screening Criteria

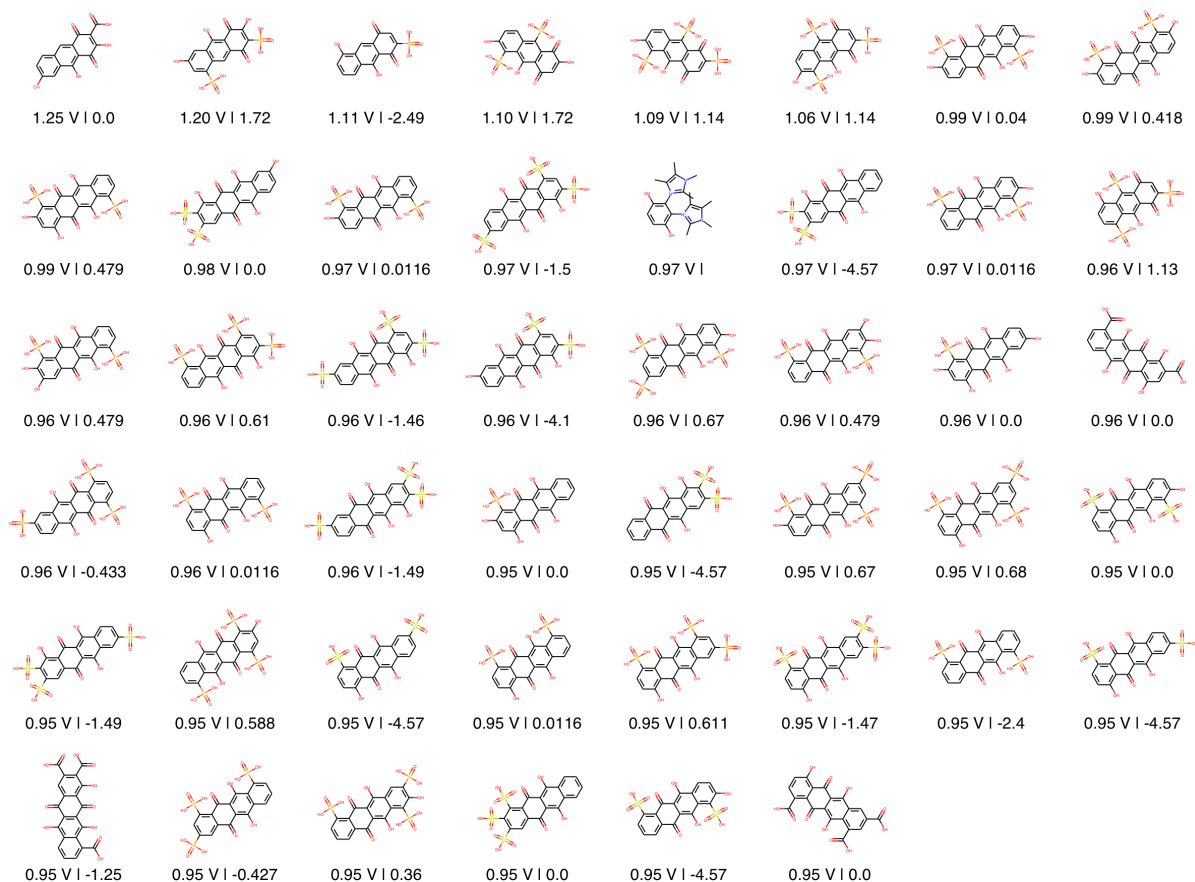


Figure S9: The reduced form of the 46 couples from the virtual screening that lack phenanthrene backbones and catechol redox topologies and have oxidized forms satisfying the following criteria: $\log K_{\text{hyd}} < 1.0$, $\Delta E_{\text{mic}} < 0.03$ eV, and reduction potentials > 0.95 V vs. SHE according to the calibrated PM7 COSMO level of theory results. The predicted potentials, based on the calibrated PM7 COSMO computations, are shown underneath each molecule (on the left). The right value under each molecule is the estimated Log (base 10) of the solubility of the (oxidized, and solubility-limiting form) molecule, calculated with ChemAxon. The calculation is only valid for molecules with no net-charge (with the exception of deprotonation). The attached screened_molecules.xlsx spreadsheet also includes calculated solubilities at $\text{pH} = 7$ and PM7 COSMO solvation free energies.

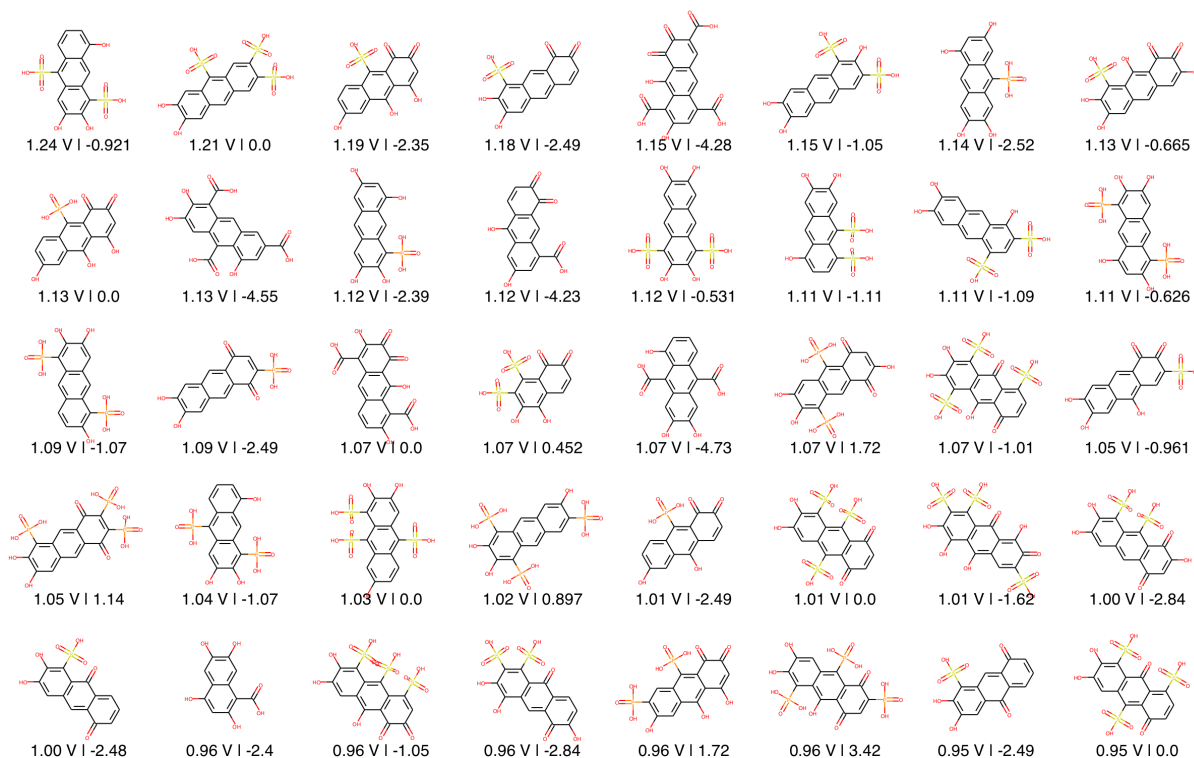


Figure S10: Sampling of the reduced forms of the 377 couples from the virtual screening that lack phenanthrene backbones and but have catechol and have oxidized forms satisfying the following criteria: $\log K_{\text{hyd}} < 1.0$, $\Delta E_{\text{mic}} < 0.03$ eV, and reduction potentials > 0.95 V vs. SHE according to the calibrated PM7 COSMO level of theory results. The predicted potentials, based on the calibrated PM7 COSMO computations, are shown underneath each molecule. Solubilities computed in the same way as above are also indicated and included in the screened_molecules.xlsx spreadsheet.

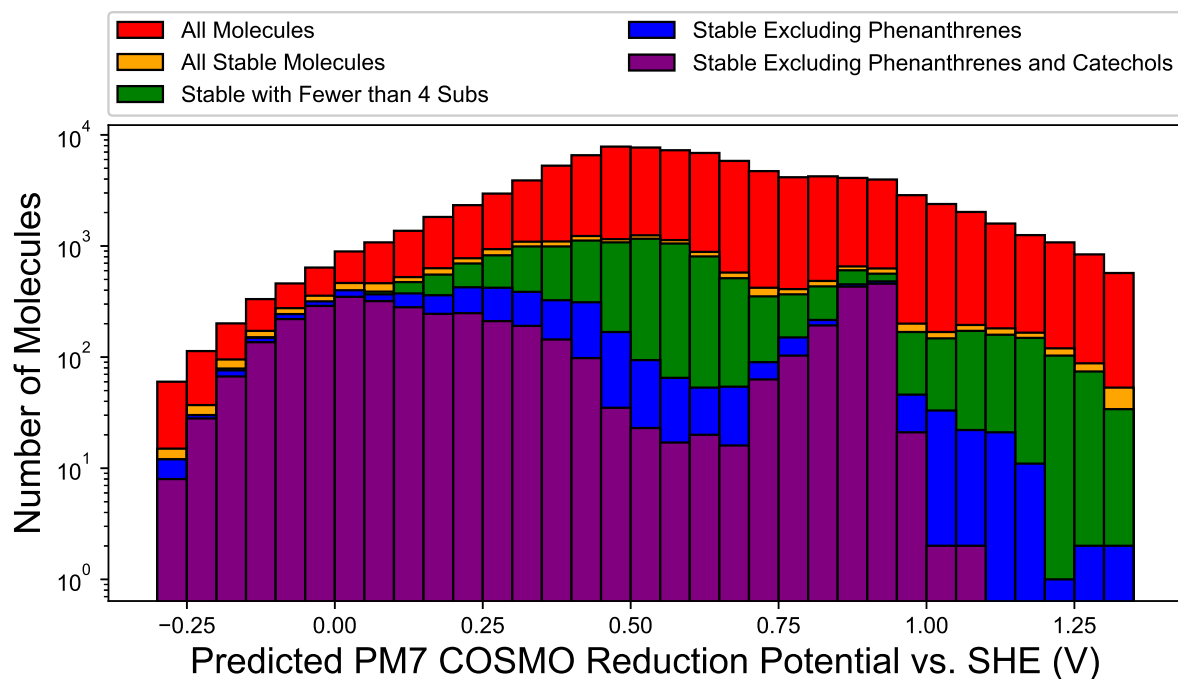


Figure S11: Plot of the reduction potential distributions of various sets of molecules, as indicated in the legend. Molecules are defined as “stable” if they have the following criteria 1) PM7 COSMO Michael addition energy < 0.00 eV and 2) $\log K_{\text{hyd}} < 0.0$. These are stricter criteria than in the main text.

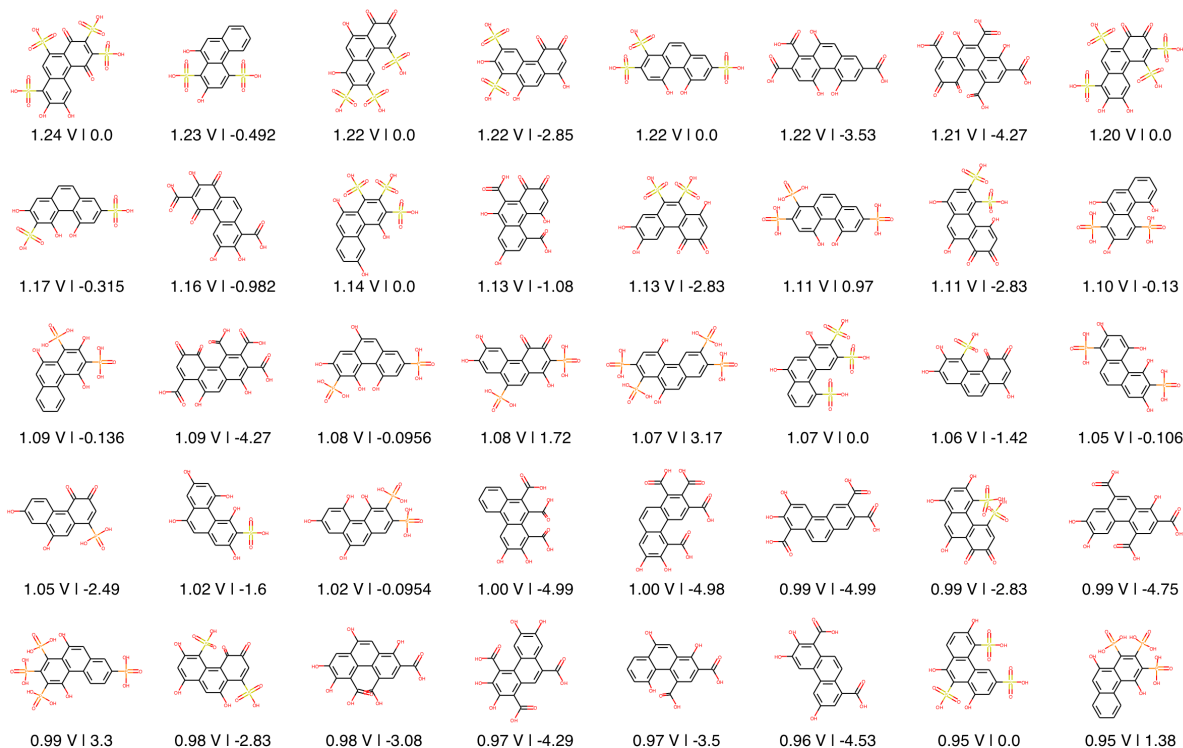
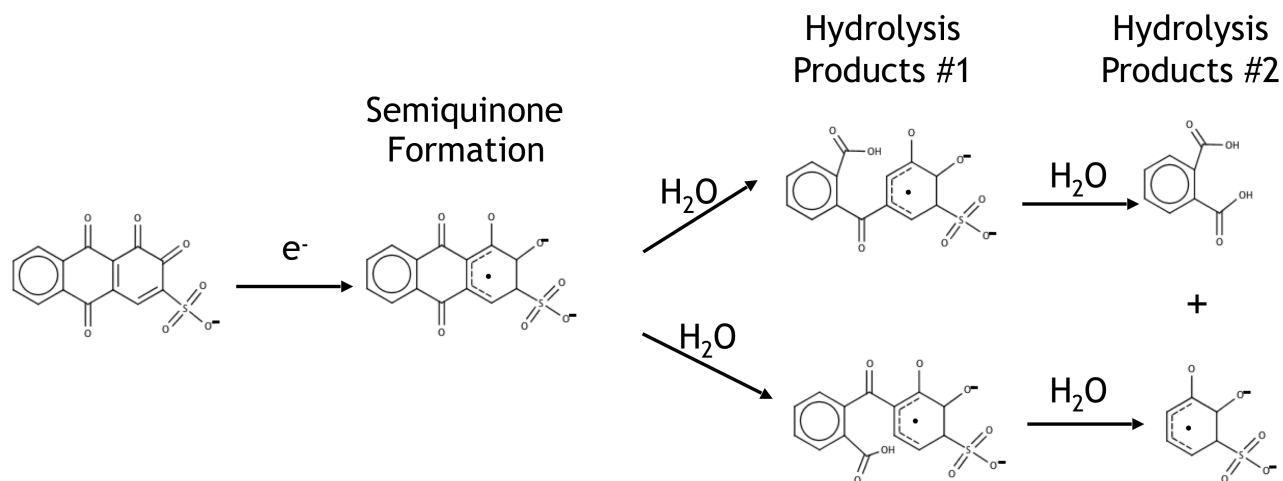


Figure S12: Sampling of the reduced forms of the 1545 couples with phenanthrene backbones that are predicted to be stable. These couples have oxidized forms with predicted $\log K_{\text{hyd}} < 1.0$ and are predicted to have reduction potentials > 0.95 V vs. SHE. These do not have a predicted Michael attack site, but are challenging to synthesize. The predicted potentials, based on the calibrated PM7 COSMO computations, are shown underneath each molecule. Solubilities computed in the same way as above are also indicated and included in the screened_molecules.xlsx spreadsheet.

S7 Potential Ring Opening Decomposition Mechanism



Scheme S1: Potential semiquinone-initiated ring-opening decomposition. This scheme is inspired by an analogous mechanism previously proposed by Yamamoto *et al.* for alizarin red S in the presence of hydrogen peroxide.^{S5} In this case, the nucleophile is water (as opposed to the hydroxide anion) and the radical source comes from electrochemical cycling (as opposed to hydrogen peroxide).

References

- [S1] Lin, K.; Gómez-Bombarelli, R.; Beh, E. S.; Tong, L.; Chen, Q.; Valle, A.; Aspuru-Guzik, A.; Aziz, M. J.; Gordon, R. G. A redox-flow battery with an alloxazine-based organic electrolyte. *Nat. Energy* **2016**, *1*, 16102.
- [S2] Er, S.; Suh, C.; Marshak, M. P.; Aspuru-Guzik, A. Computational Design of Molecules for an All-quinone Redox Flow Battery. *Chem. Sci.* **2015**, *6*, 885–893.
- [S3] Gómez-Bombarelli, R.; González-Pérez, M.; Pérez-Prior, M. T.; Calle, E.; Casado, J. Computational Calculation of Equilibrium Constants: Addition to Carbonyl Compounds. *J. Phys. Chem. A* **2009**, *113*, 11423–11428.
- [S4] J. Bingham, S.; H. P. Tyman, J. The Synthesis of Kermesic acid and Isokermesic Acid Derivatives and of Related Dihydroxyanthraquinones. *J. Chem. Soc., Perkin Trans. 1* **1997**, 3637–3642.

- [S5] Yamamoto, N.; Kubozono, T.; Kinoshita, Y. Mechanism for Oxidative Decomposition of Anthraquinone Dye with Hydrogen Peroxide. *Journal of Oleo Science* **2001**, *50*, 507–513.